Au/SiO_2 Nanoring Plasmon Waveguides at Optical Communication Band

Kyung-Young Jung, *Student Member, IEEE*, Fernando L. Teixeira, *Senior Member, IEEE*, and Ronald M. Reano, *Senior Member, IEEE*

***Abstract*—We design and investigate plasmon waveguides based on linear arrays of Au nanorings in an SiO_2 host for use in an optical communication band ($\lambda \sim 1550$ nm). Nanoring particles have better tunability and can achieve more laterally compact waveguides, compared to their solid counterparts, such as nanospheres and nanodisks. Three-dimensional simulations employing the finite-difference time-domain algorithm are used to determine the set of geometrical parameters attaining localized surface plasmon resonance at 1550 nm. It is found out that, in the SiO_2 host, Au nanorings attain LSPR at 1550 nm with a 175-nm inner diameter, a 35-nm height, and a 30-nm thickness. It is shown that linear chains of Au nanorings can transport the electromagnetic energy at 1550 nm, with transmission losses $\gamma_T = 3$ dB/655 nm and $\gamma_L = 3$ dB/443 nm and group velocities $v_{gT} = 0.177c_0$ and $v_{gL} = 0.327c_0$ for transverse and longitudinal polarizations, respectively, where c_0 is the speed of light in a vacuum.**

***Index Terms*—Finite-difference time-domain (FDTD) methods, metal nanoparticle, nanophotonics, optical communication, plasmonics.**

I. Introduction

THE electrodynamic properties of subwavelength-sized metallic nanoparticles have been extensively investigated in the past [1], [2]. It is well known that localized surface plasmon resonance (LSPR) due to coherent electron oscillations that are excited at metal–dielectric interfaces yields highly localized field enhancement and can provide guidance and confinement of electromagnetic waves below the diffraction limit. The significant enhancement of fields near metallic nanoparticles has been exploited, for example, in surface-enhanced Raman spectroscopy [3], [4], near-field optical microscopy [5], [6], and, more recently, biological sensing [7], [8]. For the latter one, the ability to sense a surrounding material is based on the high dependence of LSPR on the optical properties of the dielectric background media around metallic nanoparticles.

Plasmon waveguides based on an ordered array of metallic nanoparticles have attracted much interest [9]–[21]. Plasmon waveguides transport electromagnetic energy below the diffraction limit via near-field coupling [10]–[16] between closely spaced nanoparticles. Plasmon waveguides have been analyzed using extended Mie theory [9], point dipole models [11], multipole models [18], and finite-difference time-domain (FDTD) simulations [22]. Most previous works have considered plasmon waveguides operating at the ultraviolet or visible spectrum.

In this paper, we design and investigate plasmon waveguides to operate at wavelengths $\lambda \sim 1550$ nm (optical communication band). LSPR must be red-shifted in order to make plasmon waveguides possible at 1550 nm. Previous works have shown that the optical response of metallic nanoparticles depends on the size and shape of particles and surrounding materials [1], [8]. Using the quasi-static approximation (Rayleigh theory) [23], it is easy to show that in order to provide LSPR near 1550 nm, Au nanospheres must be surrounded by a host medium with relative permittivity as high as 55, which is not practical. Therefore, better candidates should be sought among nanoparticles with extra degrees of freedom (DoFs) in their geometry, such as nanodisks and nanorings. In the former case, the plasmon resonance can be further tuned by modifying the ratio of the longest axis (diameter) to the shortest axis (height) or by changing the radial thickness. Our numerical modeling has shown that LSPR at $\lambda = 1550$ nm occurs for Au nanodisks with 340-nm diameter and 35-nm height in the SiO_2 host. Due to their cylindrical structure, both nanodisks and nanorings allow for microfabrication techniques based on electron beam lithography (EBL). As an example, Fig. 1 shows scanning electron micrographs (SEMs) of arrays of metallic nanodisks with various diameters and interelement spacings that were fabricated in our laboratory. The fabrication process employs EBL, followed by a metal liftoff. Initially, polymethyl methacrylate with a molecular weight of 950 k is spin-coated on a blank silicon wafer with 2 μm of thermal silicon dioxide. The initial resist thickness is approximately 100 nm. The exposed resist is developed in a solution of methyl-isobutyl-ketone/isopropyl alcohol (IPA) and then rinsed in IPA. After a brief exposure to an oxygen plasma, 5 nm of Ti and 30 nm of Ni are deposited on the sample by electron beam evaporation. The initial titanium layer is used for adhesion. Metal liftoff is conducted using heated Baker PRS-2000. A similar process is applicable to other truncated cylindrical geometries, including the metallic nanorings that were considered in this paper. Compared to nanodisks, nanorings allow for further size reduction and better tunability because of the extra DoF in the geometry. LSPR in nanorings can be tuned by changing 1) the radial thickness; 2) the outer diameter; or 3) the height. The electromagnetic coupling between the inner and outer ring surfaces plays an

Manuscript received January 24, 2007; revised May 21, 2007. This work was supported in part by Air Force Office of Scientific Research under Multidisciplinary University Research Initiative Grant FA 9550-04-1-0359, by the National Science Foundation under Grant ECS-0347502, and by Ohio Supercomputer Center (OSC) under Grant PAS-0061 and Grant PAS-0110.

The authors are with the ElectroScience Laboratory and the Department of Electrical and Computer Engineering, The Ohio State University, Columbus, OH 43212 USA (e-mail: jung.166@osu.edu; teixeira@ece.osu.edu; reano@ece.osu.edu).

Color versions of one or more of the figures in this paper are available online at http://ieeexplore.ieee.org.

Digital Object Identifier 10.1109/JLT.2007.902100

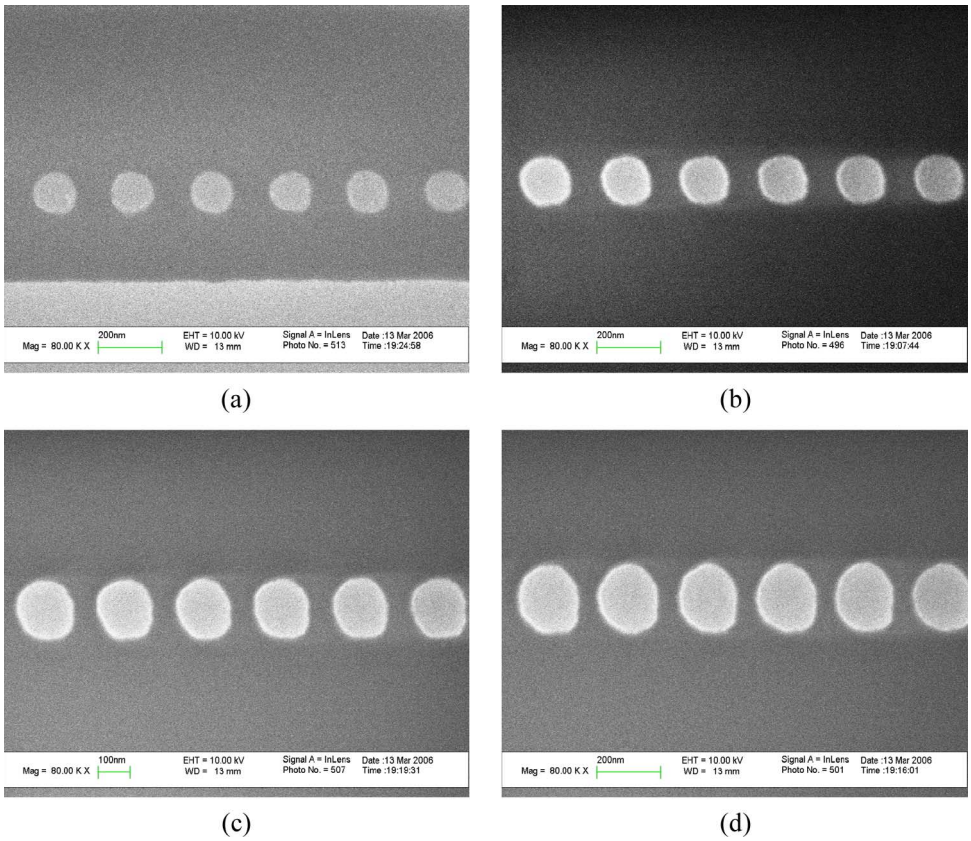

Fig. 1. SEMs of metallic nanodisks arrays with various diameters and interelement spacings. The EBL fabrication process is applicable to both the metallic nanodisks and nanorings that were discussed in this paper. (a) $D = 135$ nm, $s = 105$ nm. (b) $D = 160$ nm, $s = 95$ nm. (c) $D = 185$ nm, $s = 65$ nm. (d) $D = 195$ nm, $s = 60$ nm.

important role in optical plasmon resonance in this case [24], similarly to nanoshells [25]–[29].

The analysis and design of metallic nanorings with LPSR at 1550 nm are performed here by means of a custom 3-D FDTD algorithm that is described in the Appendix. FDTD is suited for modeling plasmon resonances and energy transport in chains of nanoparticles because of its geometrical flexibility and matrix-free (explicit update) nature. FDTD has been successfully employed to analyze a variety of structures including nanospheres [14], [17], [30], nanoellipsoids [14], nanorods [31], nanocylinders [32], nanocubes [33], nanoholes [34], and nanoshells [25]. In particular, Maier *et al.* [14] successfully applied FDTD to calculate nanosphere-based plasmon waveguide characteristics such as transmission loss and group velocity.

The remainder of this paper is organized as follows: Optical properties of an isolated Au nanoring are studied in Section II. In Section III, numerical simulations illustrate the main characteristics of plasmon waveguide based on an ordered array of Au nanorings. Concluding remarks are provided in Section IV. The present FDTD algorithm is briefly discussed in the Appendix.

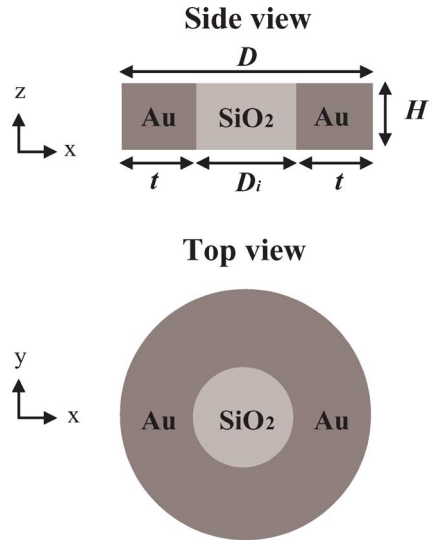

Fig. 2. Schematic illustration showing a Au nanoring surrounded by SiO_2 (core, substrate, and host medium). The three independent geometrical parameters t (metallic thickness), D_i (inner diameter), and H (height) are indicated in the side view.

II. Plasmon Resonances of Isolated Au Nanoring in SiO_2 Host

We first consider the optical resonance properties of an isolated Au nanoring, as depicted in Fig. 2, using the FDTD algorithm described in the Appendix. Fig. 2 shows the basic geometrical parameters: metallic thickness t, inner/core diameter D_i, outer diameter D, and height H. The Au nanoring is surrounded by SiO_2 (in the core, substrate, and host medium). The Au nanoring particle is excited by a plane-wave with modulated Gaussian pulse in time. We first investigate the LSPR behavior under variations on the inner diameter while setting

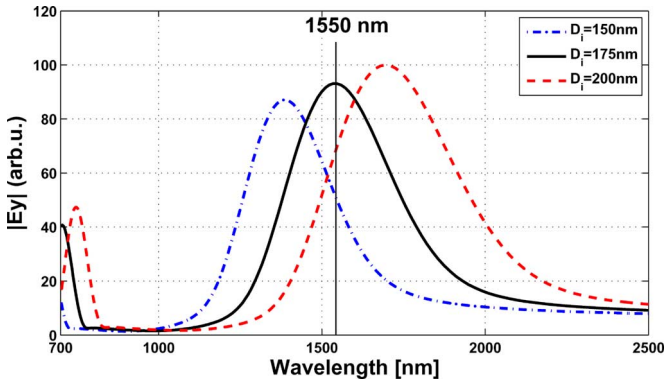

Fig. 3. Effect of inner diameter D_i on Au nanoring optical response. LSPR is red-shifted by increasing D_i. In other words, LSPR is red-shifted by increasing the ratio between the longest axis (diameter) and the shortest axis (height) of the structure.

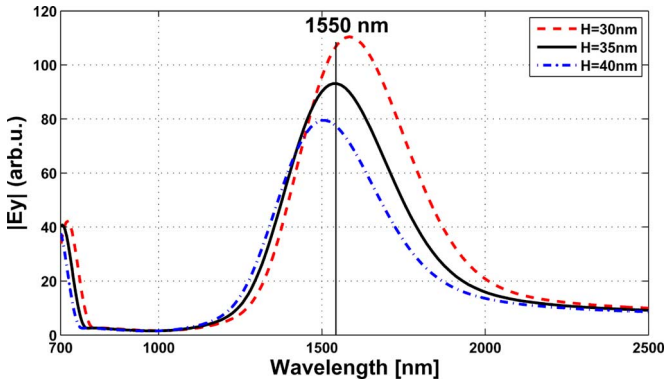

Fig. 4. Effect of height H on Au nanoring optical response. LSPR is red-shifted by decreasing t. This effect is consistent with Fig. 3, where a larger axial ratio red shifts the LSPR.

$t = 30$ nm and $H = 35$ nm fixed (to compare with the nanodisk case that was alluded to in Section I). Fig. 3 shows that a Au nanoring with an inner diameter of 175 nm leads to a plasmon resonance at 1550 nm. In this case, $D = 235$ nm, which is less than the diameter of the nanodisk (340 nm), leads to LSPR at the same wavelength.[1]

Next, we investigate the sensitivity of the plasmon resonance to variations on inner diameter, height, and thickness. For each case, one geometrical parameter is changed within $\sim$15%, while the others are fixed. Fig. 3 shows the influence of D_i on the optical response. The LSPR is red-shifted by increasing D_i. Two distinct plasmon resonances are observed at visible ($\sim$700 nm) and infrared ($\sim$1550 nm) regions of the optical spectrum. This plasmon hybridization [29] is caused by the interaction between the "cavity" [29] and "disk" [24] plasmons, which is analogous to what occurs in nanoshells. Fig. 4 shows the effect of H on the optical response. The LSPR is red-shifted by decreasing H. The dependence of the optical response on D_i and H is somewhat similar to that of a spheroidal particle. Applying a quasi-static approximation [23] to a spheroidal particle, it can be verified that the LSPR is red-shifted by increasing the eccentricity. Similarly, LSPR is shifted to longer wavelengths by increasing the diameter-to-height ratio of the nanoring. We also evaluate the change in the plasmon resonance due to variations in t, as shown in Fig. 5. The LSPR is red-shifted by decreasing t, which is akin again to the behavior of a nanoshell. Comparing Figs. 3–5, we observe that, for similar parameter deviations of about 15% at the LSPR resonance, the spectrum is considerably more sensitive to D_i than to H or t. This suggests the use of D_i as the first parameter of choice for tunability purposes.

We next examine the interplay among the geometrical parameters. First, we illustrate the interplay of D_i and t for fixed

[1]These geometrical parameters are not unique in yielding a plasmon resonance at 1550 nm since the resonance frequency is determined by a combination of geometrical parameters and surrounding medium permittivity.

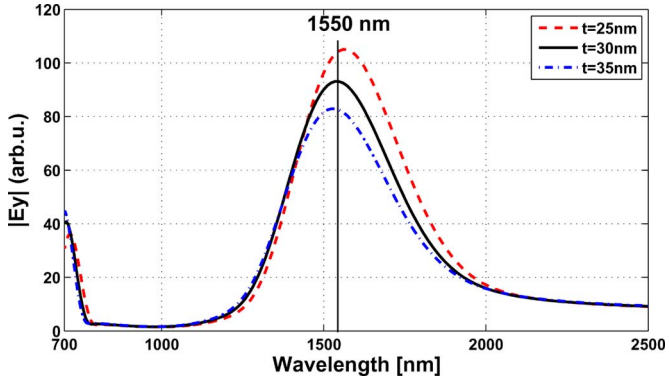

Fig. 5. Effect of thickness t on Au nanoring optical response. LSPR is red-shifted as t decreases, which is akin to what is observed in nanoshells.

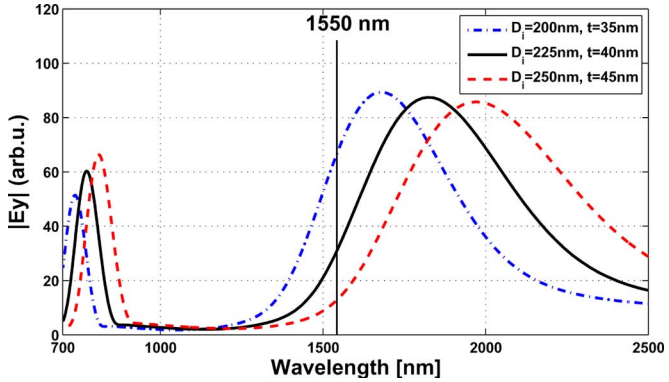

Fig. 6. Effect of simultaneous variations of inner diameter D_i and thickness t on Au nanoring optical response. LSPR is red-shifted as both D_i and t increase under similar fractional changes.

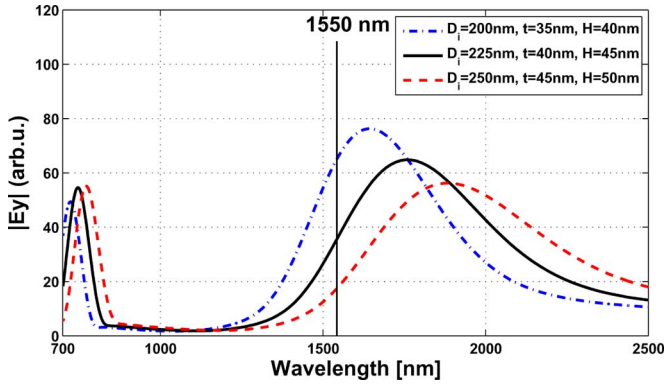

Fig. 7. Effect of simultaneous variations of inner diameter D_i, thickness t, and height H on Au nanoring optical response. LSPR is red-shifted as D_i, t, and H are increased simultaneously under similar fractional changes.

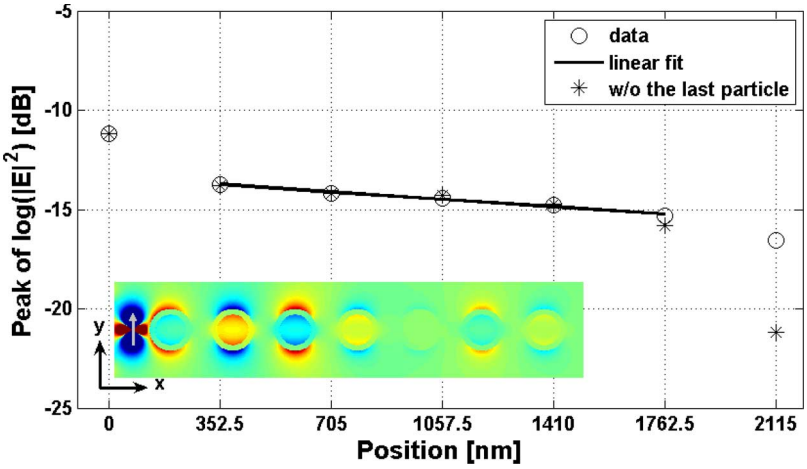

Fig. 8. Field intensity (circles) along a linear chain with seven nanoring particles under T-mode excitation. A linear fit is used to calculate the transmission loss. The field intensity along a shorter array (missing the seventh nanoring) is indicated by stars. In addition, shown in the inset is a snapshot of the E_y distribution, with polarization indicated by a gray arrow.

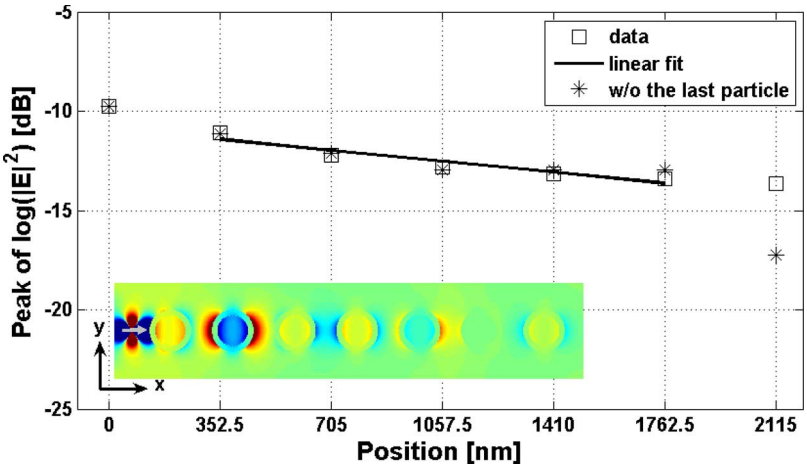

Fig. 9. Field intensity (squares) along a linear chain with seven nanoring particles under L-mode excitation. A linear fit is used to calculate the transmission loss. The field intensity along a shorter array (missing the seventh nanoring) is indicated by stars. In addition, shown in the inset is a snapshot of the E_x distribution, with polarization indicated by a gray arrow.

$H(= 35$ nm). From Figs. 3 and 5, it is known that the LSPR is red-shifted or blue-shifted by increasing D_i or t, respectively. Fig. 6 shows that the LSPR is red-shifted by increasing both D_i and t simultaneously. Compared to the case with D_i increase only, the red shift on the LSPR is reduced due to the influence of t. Fig. 7 shows results when D_i, t, and H are all increased simultaneously for three value sets. The red shift on the LSPR is smaller in this case compared with Fig. 7. Although an increase on only t or H would produce a blue shift on the LSPR, the LSPR is still red-shifted in Fig. 7 because of the stronger effect from the increase on D_i. This again illustrates that the resonance is more sensitive to (same fractional) variations on D_i.

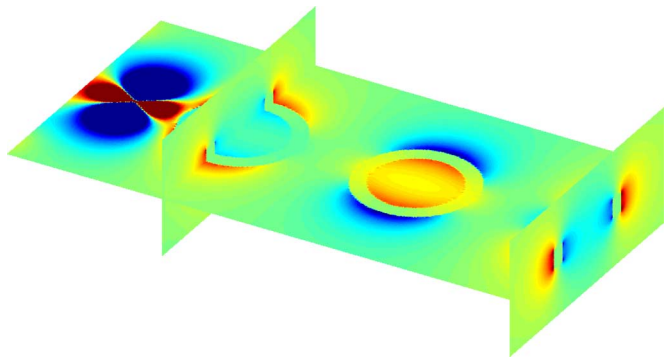

Fig. 10. Three-dimensional sliced plot of the E_y field distribution under T-mode excitation. The field is highly localized at metal–dielectric interfaces and confined transversely.

III. Plasmon Waveguides Based on Ordered Arrays of Au/SiO_2 Nanorings

We next analyze optical pulse propagation in plasmon waveguides based on ordered arrays of Au nanorings in SiO_2 host with $D_i = 175$ nm, $H = 35$ nm, and $t = 30$ nm. Seven nanoring particles with an intercenter distance of 352.5 nm $(= 1.5D)$ are located along the x-axis, forming a linear array. To study electromagnetic energy transport, noncollective modes with wavenumber $\mathbf{k} \neq 0$ need to be excited (instead of collective modes with $\mathbf{k} = 0$) [14]. To excite noncollective modes, a point dipole source is placed $1.5D$ away from the center of the first nanoring, with effective bandwidth in the

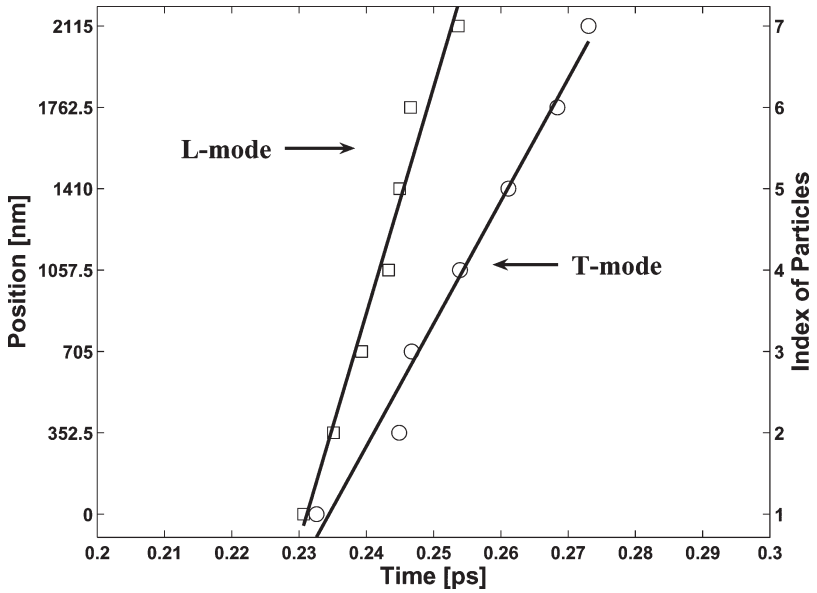

Fig. 11. Amplitude peak positions over time along a linear nanoring waveguide. Note the faster group velocity for the L mode compared to that of the T mode.

range of 1530–1570 nm. We set the center of the first nanoring at reference position 0 nm.

Plasmon waveguides are lossy, and to examine the transmission loss, we calculate the field intensity along the linear chain when excited by a dipole pulse with transverse (T-mode) or longitudinal (L-mode) polarizations (with respect to the chain axis). Figs. 8 and 9 show the logarithm of the peak amplitude squared of the electric field along the plasmon waveguide for the T and L modes, respectively. In addition, shown in the inset are snapshots of E_y for the T mode and E_x for the L mode along the nanochain. The polarization is indicated by a gray arrow. The field intensity shown is calculated by averaging the square of electric fields over the outer surface of nanoring. Due to impedance mismatch [9], reflections are observed at the first and last nanorings, and hence, these values are excluded when interpolating the values along the plasmon waveguide. As the pulse propagates along the waveguide, the field intensity decays in an exponential fashion, i.e., $|E|^2 \propto \exp(-\gamma x)$ [9]. The transmission loss is extracted by fitting the data (indicated by circles or squares) with a linear fit in the log scale. The transmission loss factors for the T and L modes are $\gamma_T = 3$ dB$/655$ nm and $\gamma_L = 3$ dB$/443$ nm, respectively. We also display the field intensity (indicated by stars) along a shorter array missing the seventh nanoring. To illustrate the field confinement on the transverse direction, we show a 3-D sliced plot of the E_y field distribution (T mode) in Fig. 10, where it is observed that the fields are highly localized at metal–dielectric interfaces and confined transversely.

Next, we determine the group velocity by tracking the amplitude peak positions over time, as shown in Fig. 11. The group velocities for T mode (v_{g_T}) and L mode (v_{g_L}) are found to be about $0.177c_0$ and $0.327c_0$, respectively, where c_0 is the speed of light in a vacuum. Note the faster group velocity of L mode compared to that of T mode, which is akin to the nanosphere plasmon waveguide case [14]. The influence of interelement spacing on both the propagation loss and the group velocity is shown in Fig. 12. The three interelement spacings that were considered (0, 117.5, and 235 nm) correspond to intercenter distances D, $1.5D$, and $2D$, respectively. The interelement spacing of 0 nm corresponds to successive nanorings that touch each other. For the T mode, the 3-dB intensity decay length decreases as the intercenter distance increases. On the other hand, for the L mode, the 3-dB intensity decay length is maximum for an intercenter distance of $1.5D$. Fig. 12 also shows that the intercenter distance of $1.5D$ supports the fastest (slowest) group velocity for the L mode (T mode).

The potential for subwavelength routing and switching of optical pulses is one of the major appeals of plasmon waveguides [11], [21]. L-junction (90° sharp bend) structures that are composed of seven nanorings (three nanorings in both horizontal and vertical arms, and one nanoring at the junction position) are analyzed under T-mode excitation. Note that a T-mode excitation is converted into L mode through L-junctions, and vice versa. Comparison of (time-averaged) the field amplitude around the last nanoparticle between this bending structure and the linear chain leads to a bending loss of 7.3 dB. The transmission performance for 90° bends (zero radius of curvature) in nanoring plasmon waveguides is worse than those in metal–dielectric–metal plasmon waveguides [35] and in photonic crystal waveguides [36] but better than that in dielectric rib waveguides [37]. Fig. 13 shows a snapshot of the E_y field along the L-junction. As can be seen, the electric field is guided along the horizontal arm and coupled into the vertical arm.

We next illustrate the coherent interference of two plasmon–polariton waves that are excited with different phases. The operation of optical switches can be based on such interference [21]. A linear chain that is composed of seven nanorings is excited at both ends with oscillating dipole sources either in-phase ("constructive" interference) or 180° off-phase ("destructive" interference). Fig. 14 displays snapshots of the E_y field distribution along the linear chain, showing the interference of two plasmon–polariton waves. One can observe that the E_y

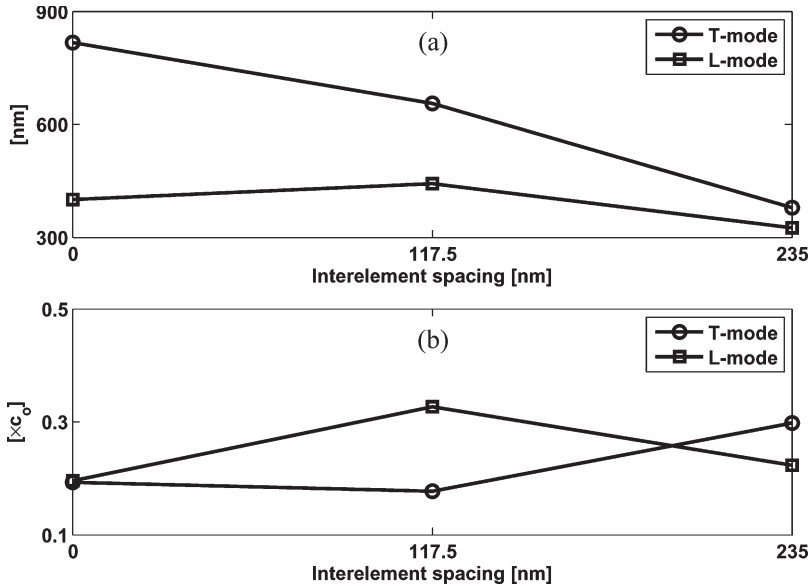

Fig. 12. Influence of interelement spacing on propagation characteristics. (a) 3-dB intensity decay length. (b) Group velocity.

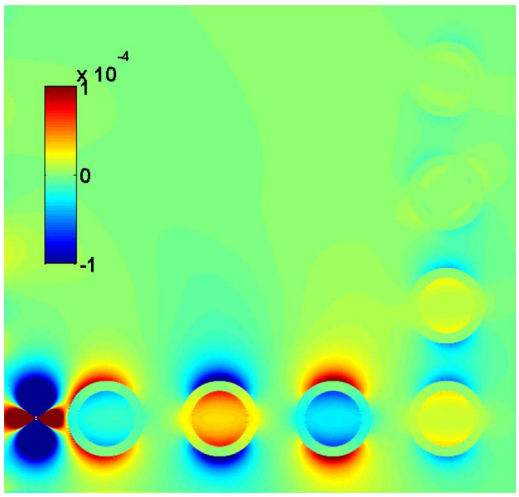

Fig. 13. Snapshot of E_y under T-mode excitation. The electric field is guided along the horizontal arm and coupled into the vertical arm with the bending loss of 7.3 dB.

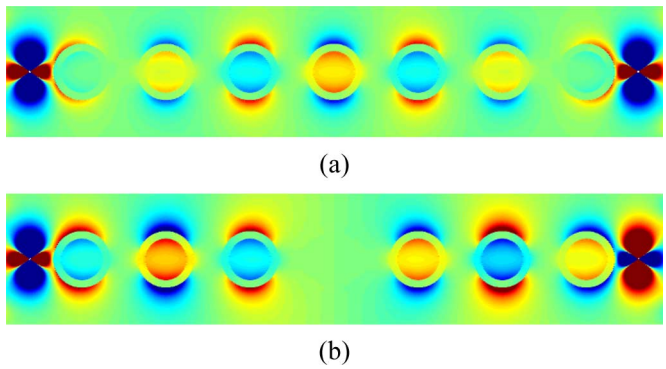

Fig. 14. Interference of two plasmon–polariton waves under T-mode excitation. The comparison between two snapshots of the E_y field provides the evidence of coherent interference of two plasmon–polariton waves. Two dipole sources are employed with either (a) in-phase or (b) out-of-phase excitation. (a) Constructive interference and (b) destructive interference.

field is symmetrically or antisymmetrically distributed along the y plane of the center (fourth) particle under constructive or destructive interferences, respectively.

IV. Summary and Conclusion

Plasmon waveguides that are based on ordered arrays of Au nanorings in an SiO_2 host have been designed and investigated for use in an optical communication band. The analysis was performed by a complex frequency shifted–perfectly matched layer–FDTD algorithm that accounts for the monospecies Drude dispersion model of Au at the frequencies that were considered and effectively suppresses spurious reflections from both propagating and evanescent waves on the computational grid boundaries. This leads to a decrease in the computational cost as the computational boundary can be closely placed near the nanoparticles. Furthermore, in order to reduce staircasing error, a field-centered approach was employed to model the material properties that better conform to the curved metal-to-dielectric interfaces.

The optical properties of an isolated Au nanoring were studied to determine the set of geometrical parameters producing LSPR at 1550 nm (optical communication band). It has been found that a nanoring with 175-nm inner diameter, 30-nm metallic thickness, and 35-nm height in the SiO_2 host produces LSPR at the desired wavelength. The transmission loss and group velocity were calculated for both T- and L-polarized pulses. The L mode was found to be more lossy and have a faster group velocity than the T mode. The effect of the intercenter distance between nanorings on propagation characteristics was also considered. For the interelement distances that were considered, a spacing of about 120 nm has produced the faster group velocity and smaller loss for the L mode. For the T mode, the loss was found to increase with the interelement distance, being minimal for adjoining particles. Finally, more complex structures such as an L-junction and a linear chain with two driving dipole sources were also considered and simulated to further illustrate the guiding properties of nanoring

chains and the coherent interference of two plasmon pulses with opposite directions of propagation.

APPENDIX
FDTD ALGORITHM FOR PLASMONICS

At the wavelengths of interest, the (complex) relative permittivity of Au is described by a monospecies Drude dispersion model given by

$$\epsilon_r(\omega) = \epsilon_\infty - \frac{\omega_p^2}{\omega^2 + i\Gamma\omega} \tag{1}$$

where ω_p is the plasma frequency, and Γ is the damping coefficient, with $\epsilon_\infty = 9.5$, $\omega_p = 8.9488$ eV, and $\Gamma = 0.06909$ eV [25], [38]. From the preceding equation, 3-D FDTD update equations can be derived in a standard fashion [32], [39], [40], with the accuracy mainly dictated by truncation and grid dispersion error. Modified finite differences can also be easily implemented to yield low *grid* dispersion error over prescribed frequency ranges [41]. It should be pointed out that a multispecies Drude–Lorentz dispersion model (rather than monospecies Drude only) becomes necessary when the wavelength range of interest is below 700 nm due to interband transitions [31], [42]. However, we use the monospecies Drude model in our study, because the prescribed wavelength range is out of the wavelength range that is influenced by interband transitions. The refractive index of SiO_2 deviates from the nominal value within 1% in the wavelength range between 590 and 2500 nm [43]. Hence, we use the nominal value 1.44 in all simulations. We use a coordinate-dependent permittivity $(\epsilon_x, \epsilon_y, \epsilon_z)$ that is associated with each electric field component (E_x, E_y, E_z) (field-centered), rather than assign a single-valued permittivity to a whole unit cell (cell-centered) [44]. For example, the finite-difference update equations for Ampere's law in the dielectric regions are given by

$$\begin{aligned} E^{n+1}_{x_{i+1/2,j,k}} &= E^{n}_{x_{i+1/2,j,k}} \\ &+ \frac{\Delta t}{\epsilon_{i+1/2,j,k}} \left[\frac{H^{n+1/2}_{z_{i+1/2,j+1/2,k}} - H^{n+1/2}_{z_{i+1/2,j-1/2,k}}}{\Delta y} \right] \\ &- \frac{\Delta t}{\epsilon_{i+1/2,j,k}} \left[\frac{H^{n+1/2}_{y_{i+1/2,j,k+1/2}} - H^{n+1/2}_{y_{i+1/2,j,k-1/2}}}{\Delta z} \right] \end{aligned} \tag{2}$$

$$\begin{aligned} E^{n+1}_{y_{i,j+1/2,k}} &= E^{n}_{y_{i,j+1/2,k}} \\ &+ \frac{\Delta t}{\epsilon_{i,j+1/2,k}} \left[\frac{H^{n+1/2}_{x_{i,j+1/2,k+1/2}} - H^{n+1/2}_{x_{i,j+1/2,k-1/2}}}{\Delta z} \right] \\ &- \frac{\Delta t}{\epsilon_{i,j+1/2,k}} \left[\frac{H^{n+1/2}_{z_{i+1/2,j+1/2,k}} - H^{n+1/2}_{zi-1/2,j+1/2,k}}{\Delta x} \right] \end{aligned} \tag{3}$$

$$\begin{aligned} E^{n+1}_{z_{i,j,k+1/2}} &= E^{n}_{z_{i,j,k+1/2}} \\ &+ \frac{\Delta t}{\epsilon_{i,j,k+1/2}} \left[\frac{H^{n+1/2}_{y_{i+1/2,j,k+1/2}} - H^{n+1/2}_{y_{i-1/2,j,k+1/2}}}{\Delta x} \right] \\ &- \frac{\Delta t}{\epsilon_{i,j,k+1/2}} \left[\frac{H^{n+1/2}_{x_{i,j+1/2,k+1/2}} - H^{n+1/2}_{x_{i,j-1/2,k+1/2}}}{\Delta y} \right] \end{aligned} \tag{4}$$

where the subscript refers to spatial grid indexing, and the superscript refers to the time step. Such coordinate-dependent permittivity is also used for the dispersive models in metallic regions. Although this field-centered approach requires three times more unknowns for the permittivity than the cell-centered approach in isotropic media, it does a better job of conforming to material boundaries and, hence, reducing the staircasing error of FDTD [44].

To minimize spurious reflections from the outer boundary of the computational domain, the perfectly matched layer is incorporated through a modified nabla operator with complex stretching coordinates [45]–[48], where complex-frequency shifted stretching [49]–[51] is utilized. In all simulations, we use a mesh cell size of 2.5 nm and a Courant factor of 0.95. The simulations were performed on a Cray X1 using one multistreaming processor with four 800-MHz internal processors. The FDTD grid comprised $1080 \times 236 \times 114$ nodes for a total of 5.4×10^8 unknowns for the seven-nanoring chain example, requiring about 42.5 h of computation time for a 5×10^{-13} s time window. The L-junction example employed $657 \times 617 \times 114$ nodes, for a total of 8.4×10^8 unknowns, requiring about 71.6 h for a 5×10^{-13} s time window.

REFERENCES

[1] U. Kreibig and M. Vollmer, *Optical Properties of Metal Clusters*. Berlin, Germany: Springer-Verlag, 1995.

[2] V. M. Shalaev, *Optical Properties of Nanostructured Random Media*. Berlin, Germany: Springer-Verlag, 2002.

[3] S. Nie and S. R. Emory, "Probing single molecules and single nanoparticles by surface-enhanced Raman scattering," *Science*, vol. 275, no. 5303, pp. 1102–1106, Feb. 1997.

[4] H. Xu, E. J. Bjerneld, M. Käll, and L. Börjesson, "Spectroscopy of single hemoglobin molecules by surface enhanced Raman scattering," *Phys. Rev. Lett.*, vol. 83, no. 21, pp. 4357–4360, Nov. 1999.

[5] H. Heinzelmann and D. W. Pohl, "Scanning near-field optical microscopy," *Appl. Phys. A, Solids Surf.*, vol. 59, no. 2, pp. 89–101, Aug. 1994.

[6] R. M. Stockle, Y. D. Suh, V. Deckert, and R. Zenobi, "Nanoscale chemical analysis by tip-enhanced Raman spectroscopy," *Chem. Phys. Lett.*, vol. 318, no. 1, pp. 131–136, Feb. 2000.

[7] J.-M. Nam, C. S. Thaxton, and C. A. Mirkin, "Nanoparticle-based bio-bar codes for the ultrasensitive detection of proteins," *Science*, vol. 301, no. 5641, pp. 1884–1886, Sep. 2003.

[8] J. J. Mock, D. R. Smith, and S. Schultz, "Local refractive index dependence of plasmon resonance spectra from individual nanoparticles," *Nano Lett.*, vol. 3, no. 4, pp. 485–491, Apr. 2003.

[9] M. Quinten, A. Leitner, J. R. Krenn, and F. R. Aussenegg, "Electromagnetic energy transport via linear chains of silver nanoparticles," *Opt. Lett.*, vol. 23, no. 17, pp. 1331–1333, Sep. 1998.

[10] J. R. Krenn, A. Dereux, J. C. Weeber, E. Bourillot, Y. Lacroute, J. P. Goudonnet, G. Schider, W. Gotschy, A. Leitner, F. R. Aussenegg, and C. Girard, "Squeezing the optical near-field zone by plasmon coupling of

metallic nanoparticles," *Phys. Rev. Lett.*, vol. 82, no. 12, pp. 2590–2593, Mar. 1999.
[11] M. L. Brongersma, J. W. Hartman, and H. A. Atwater, "Electromagnetic energy transfer and switching in nanoparticle chain arrays below the diffraction limit," *Phys. Rev. B, Condens. Matter*, vol. 62, no. 24, pp. R16 356–R16 359, Dec. 2000.
[12] S. A. Maier, M. L. Brongersma, P. G. Kik, S. Meltzer, A. A. G. Requicha, and H. A. Atwater, "Plasmonics—A route to nanoscale optical devices," *Adv. Mater.*, vol. 13, no. 19, pp. 1501–1505, Oct. 2001.
[13] S. A. Maier, P. G. Kik, and H. A. Atwater, "Observation of coupled plasmon-polariton modes in Au nanoparticle chain waveguide of different lengths: Estimation of waveguide loss," *Appl. Phys. Lett.*, vol. 81, no. 9, pp. 1714–1716, Aug. 2002.
[14] S. A. Maier, P. G. Kik, and H. A. Atwater, "Optical pulse propagation in metal nanoparticle chain waveguides," *Phys. Rev. B, Condens. Matter*, vol. 67, no. 20, p. 205 402, May 2003.
[15] S. A. Maier, M. L. Brongersma, P. G. Kik, and H. A. Atwater, "Observation of near-field coupling in metal nanoparticle chains using far-field polarization spectroscopy," *Phys. Rev. B, Condens. Matter*, vol. 65, no. 19, p. 193 408, May 2002.
[16] S. A. Maier, P. G. Kik, H. A. Atwater, S. Meltzer, E. Harel, B. E. Koel, and A. A. G. Requicha, "Local detection of electromagnetic energy transport below the diffraction limit in metal nanoparticle plasmon waveguides," *Nat. Mater.*, vol. 2, no. 4, pp. 229–232, Apr. 2003.
[17] L. A. Sweatlock, S. A. Maier, H. A. Atwater, J. J. Penninkhof, and A. Polman, "Highly confined electromagnetic field in arrays of strongly coupled Ag nanoparticles," *Phys. Rev. B, Condens. Matter*, vol. 71, no. 23, p. 235 408, Jun. 2005.
[18] S. Y. Park and D. Stroud, "Surface-plasmon dispersion relations in chains of metallic nanoparticles: An exact quasistatic calculation," *Phys. Rev. B, Condens. Matter*, vol. 69, no. 12, p. 125 418, Mar. 2004.
[19] C. Girard and R. Quidant, "Near-field optical transmittance of metal particle chain waveguides," *Opt. Express*, vol. 12, no. 25, pp. 6141–6146, Dec. 2004.
[20] J. J. Xiao, J. P. Huang, and K. W. Yu, "Optical response of strongly coupled metal nanoparticles in dimer arrays," *Phys. Rev. B, Condens. Matter*, vol. 71, no. 4, p. 045 404, Jan. 2005.
[21] S. A. Maier, "Guiding of electromagnetic energy in subwavelength periodic metal structures," Ph.D. dissertation, California Inst. Technol., Pasadena, CA, 2003.
[22] A. Taflove and S. C. Hagness, *Computational Electrodynamics: The Finite-Difference Time-Domain Method*, 2nd ed. Norwood, MA: Artech House, 2000.
[23] C. F. Bohren and D. R. Huffman, *Absorption and Scattering of Light by Small Particles*. New York: Wiley, 1983.
[24] J. Aizpurua, P. Hanarp, D. S. Sutherland, M. Käll, G. W. Bryant, and F. J. García de Abajo, "Optical properties of gold nanorings," *Phys. Rev. Lett.*, vol. 90, no. 5, p. 057 401, Feb. 2003.
[25] C. Oubre and P. Nordlander, "Optical properties of metallodielectric nanostructures calculated using the finite difference time domain method," *J. Phys. Chem. B*, vol. 108, no. 46, pp. 17 740–17 747, Nov. 2004.
[26] S. J. Oldenburg, J. B. Jackson, S. L. Westcott, and N. J. Halas, "Infrared extinction properties of gold nanoshells," *Appl. Phys. Lett.*, vol. 75, no. 19, pp. 2897–2899, Nov. 1999.
[27] J. B. Jackson and N. J. Halas, "Silver nanoshells: Variations in morphologies and optical properties," *J. Phys. Chem. B*, vol. 105, no. 14, pp. 2743–2746, Apr. 2001.
[28] E. Prodan and P. Nordlander, "Structural tunability of the plasmon resonances in metallic nanoshells," *Nano Lett.*, vol. 3, no. 4, pp. 543–547, Apr. 2003.
[29] E. Prodan, C. Radloff, N. J. Halas, and P. Nordlander, "A hybridization model for the plasmon response of complex nanostructures," *Science*, vol. 302, no. 5644, pp. 419–422, Oct. 2003.
[30] W. A. Challener, I. K. Sendur, and C. Peng, "Scattered field formulation of finite difference time domain for a focused light beam in dense media with lossy materials," *Opt. Express*, vol. 11, no. 23, pp. 3160–3170, Nov. 2003.
[31] A. Vial, A.-S. Grimault, D. Macías, D. Barchiesi, and M. L. de la Chapelle, "Improved analytical fit of gold dispersion: Application to the modeling of extinction spectra with a finite-difference time-domain method," *Phys. Rev. B, Condens. Matter*, vol. 71, no. 8, p. 085 416, Feb. 2005.
[32] S. K. Gray and T. Kupka, "Propagation of light in metallic nanowire arrays: Finite-difference time-domain studies of silver cylinders," *Phys. Rev. B, Condens. Matter*, vol. 68, no. 4, p. 045 415, Jul. 2003.
[33] L. J. Sherry, S.-H. Chang, G. C. Schatz, and R. P. Van Duyne, "Localized surface plasmon resonance spectroscopy of single silver nanocubes," *Nano Lett.*, vol. 5, no. 10, pp. 2034–2038, Oct. 2005.
[34] S.-H. Chang, S. K. Gray, and G. C. Schatz, "Surface plasmon generation and light transmission by isolated nanoholes and arrays of nanoholes in thin metal films," *Opt. Express*, vol. 13, no. 8, pp. 3150–3165, Apr. 2005.
[35] G. Veronis and S. Fan, "Bends and splitters in metal-dielectric-metal subwavelength plasmonic waveguides," *Appl. Phys. Lett.*, vol. 87, no. 13, p. 1102, Sep. 2005.
[36] A. Mekis, J. C. Chen, I. Kurland, S. Fan, P. R. Villeneuve, and J. D. Joannopoulos, "High transmission through sharp bends in photonic crystal waveguides," *Phys. Rev. Lett.*, vol. 77, no. 18, pp. 3787–3790, Oct. 1996.
[37] M. Rajarajan, S. Obayya, B. Rahman, K. Grattan, and H. El-Mikati, "Characterisation of low-loss waveguide bends with offset-optimisation for compact photonic integrated circuits," *Proc. Inst. Elect. Eng.—Optoelectron.*, vol. 147, no. 6, pp. 382–388, Dec. 2000.
[38] P. B. Johnson and R. W. Christy, "Optical constants of the noble metals," *Phys. Rev. B, Condens. Matter*, vol. 6, no. 12, pp. 4370–4379, Dec. 1972.
[39] F. L. Teixeira and W. C. Chew, "Finite-difference computation of transient electromagnetic waves for cylindrical geometries in complex media," *IEEE Trans. Geosci. Remote Sens.*, vol. 38, no. 4, pp. 1530–1543, Jul. 2000.
[40] K.-Y. Jung, B. Donderici, and F. L. Teixeira, "Transient analysis of spectrally asymmetric magnetic photonic crystals with ferromagnetic losses," *Phys. Rev. B, Condens. Matter*, vol. 74, no. 16, p. 165 207, Oct. 2006.
[41] S. Wang and F. L. Teixeira, "Lattice models for large-scale simulations of coherent wave scattering," *Phys. Rev. E, Stat. Phys. Plasmas Fluids Relat. Interdiscip. Top.*, vol. 69, no. 1, p. 016 701, Jan. 2004.
[42] K.-Y. Jung and F. L. Teixeira, "Multispecies ADI-FDTD algorithm for nanoscale three-dimensional photonic metallic structures," *IEEE Photon. Technol. Lett.*, vol. 19, no. 8, pp. 586–588, Apr. 2007.
[43] E. D. Palick, *Handbook of Optical Constants of Solids*. Orlando, FL: Academic, 1985.
[44] G. W. Burr, "FDTD as a nanophotonics design optimization tool," presented at the Int. Symp. Photonic Electromagn. Crystal Structures V, Kyoto, Japan, 2004.
[45] W. M. Chew and W. H. Weedon, "A 3D perfectly matched medium from modified Maxwell's equations with stretched coordinates," *Microw. Opt. Technol. Lett.*, vol. 7, no. 3, pp. 599–604, Sep. 1994.
[46] F. L. Teixeira and W. C. Chew, "Systematic derivation of anisotropic PML absorbing media in cylindrical and spherical coordinates," *IEEE Microw. Guided Wave Lett.*, vol. 7, no. 11, pp. 371–373, Nov. 1997.
[47] F. L. Teixeira and W. C. Chew, "Analytical derivation of a conformal perfectly matched absorber for electromagnetic waves," *Microw. Opt. Technol. Lett.*, vol. 17, no. 4, pp. 231–236, 1998.
[48] F. L. Teixeira and W. C. Chew, "A general approach to extend Berenger's absorbing boundary condition to anisotropic and dispersive media," *IEEE Trans. Antennas Propag.*, vol. 46, no. 9, pp. 1386–1387, Sep. 1998.
[49] M. Kuzuoglu and R. Mittra, "Frequency dependence of the constitutive parameters of causal perfectly matched anisotropic absorbers," *IEEE Microw. Guided Wave Lett.*, vol. 6, no. 12, pp. 447–449, Dec. 1996.
[50] J. A. Roden and S. D. Gedney, "Convolution PML (CPML): An efficient FDTD implementation of the CFS-PML for arbitrary media," *Microw. Opt. Technol. Lett.*, vol. 27, no. 5, pp. 334–339, Dec. 2000.
[51] E. Becache, P. G. Petropoulos, and S. D. Gedney, "On the long-time behavior of unsplit perfectly matched layers," *IEEE Trans. Antennas Propag.*, vol. 52, no. 5, pp. 1335–1342, May 2004.

Kyung-Young Jung (S'06) was born in Seoul, Korea, in 1974. He received the B.S. and M.S. degrees in electrical engineering from Hanyang University, Seoul, in 1996 and 1998, respectively. He is currently working toward the Ph.D. degree at the ElectroScience Laboratory and the Department of Electrical and Computer Engineering, The Ohio State University, Columbus.

He was with the R&D Department, Mobile Telecommunication Terminal Division, Hyundai Electronics Industries, from 1998 to 2001 and with the R&D Laboratory, Curitel Communications, from 2001 to 2004. His research interests include numerical modeling for electromagnetic metamaterials, nanophotonics, and plasmonics.

Fernando L. Teixeira (S'96–M'00–SM'05) received the Ph.D. degree in electrical engineering from the University of Illinois at Urbana-Champaign in 1999.

From 1999 to 2000, he was a Postdoctoral Research Associate with the Research Laboratory of Electronics, Massachusetts Institute of Technology, Cambridge. Since 2000, he has been with the ElectroScience Laboratory and the Department of Electrical and Computer Engineering, The Ohio State University, Columbus, where he is currently an Associate Professor. His current research interests include analytical and numerical techniques for wave propagation and scattering problems in communication, sensing, and devices applications.

Dr. Teixeira was the recipient of many prizes for his research, including the National Science Foundation CAREER Award in 2004 and the triennial U.S.NC/URSI Booker Fellowship in 2005.

Ronald M. Reano (S'00–M'04–SM'06) received the B.S. degree in physics from the University of California, Los Angeles, in 1991, the B.S. degree in electrical engineering from the University of New Mexico, Albuquerque, in 1996, and the M.S. and Ph.D. degrees in electrical engineering from the University of Michigan, Ann Arbor, in 2000 and 2004, respectively. His doctoral research interests involved optoelectronic materials and optical measurement techniques for studying microwave- and millimeter-wave devices. His postdoctoral research was in the area of nanotechnology for biomaterials at the Solid-State Electronics Laboratory, University of Michigan.

From May 1992 to October 1996, he was with the Air Force Operational Test and Evaluation Center, Kirtland Air Force Base, NM, as an Electronic Aircraft Systems Reliability Analyst. He is currently an Assistant Professor with the Department of Electrical and Computer Engineering, The Ohio State University, Columbus.

Dr. Reano was the recipient of the 2003 Distinguished Achievement Award, Electrical Engineering Ph.D. Program, which was presented by the College of Engineering, University of Michigan; the First Place Award at the Student Paper Competition that was presented at the 2001 IEEE International MTT-S Symposium; and the 1999 Outstanding Graduate Student Instructor Award, which was presented by the Electrical Engineering and Computer Science Department, University of Michigan.